Numerical Analysis of Newtonian Fluids in Channel Flows using Semi-Implicit Time Stepping Taylor-Galerkin/Pressure Method

Rahim Bux Khokhar[*], Afaque Ahmed Bhutto[†], Iftikhar Ahmed Bhutto[‡], Fozia Shaikh[§], Muhahhamd Anwar Solangi[**]

Abstract

Taylor-Galerkin/Pressure-Correction primitive variable finite element algorithm is used to simulate Newtonian fluids in channels under diverse flow conditions. The purpose of this study is to investigate the algorithm's ability to accurately predict steady and complex flows, including bifurcations that may result as flow direction and stream rate change. For together equal and unequal stream rates, the study examines the impact of inertia on flow structure and pressure. Vortex intensity increases as Reynolds number increases, while unidirectional flow is promoted, and vortex intensity decreases as flow rate decreases. The intensity of vortex growth recirculation and pressure differences caused by changes in flow rates and directions were also measured during the study. This study aims to provide insight into Newtonian fluid behavior in a channel under varying flow conditions and demonstrate the effectiveness of the Taylor-Galerkin/Pressure-Correction finite element algorithm.

Keywords: Newtonian fluids, Steady flows, flow rate, Inertia, Vortex intensity, Reynold number.

Introduction

The study There are broad applications of the study of flows in channels in many fields, such as chemical engineering, biomedical engineering, and mechanical engineering. Unidirectional and reverse flows can characterize the behavior of Newtonian fluids in channels. Fluid transportation processes can be optimized and energy consumption reduced by understanding the dynamics of such flows (Baloch et al., 1995; Xia & Sun, 2002). The study of the movement of smooth fluids finished complicated canals and tubes occupied with porous and non-porous materials has remained a crucial and fascinating topic in the field of computational fluid dynamics (CFD), particularly in numerous industrial processing industries (Baaijens, 1998; Xia & Sun, 2002). In view of the complex flow behavior of non-linear fluids, the convoluted rheological properties of these fluids, and the complexity of the domains involved, industrial issues become increasingly difficult to address. Mathematicians and scientists are therefore stimulated and challenged by these complexities. Although several industrial scenarios are discussed in the paper, the author places a heavy emphasis on a small number of them. A variety of industries are involved in the processing of crude oil, enhanced oil recovery within the petroleum industry, ceramics, chemicals, cosmetics, dryers, filters, food, and pharmaceuticals. The author

[*]Department of BSRS, Mehran University of Engineering and Technology Jamshoro, Pakistan, rahimbux.khokhar@faculty.muet.edu.pk
[†]Department of BSRS, QUEST Campus, Larkana, Pakistan, afaq_bhutto@quest.edu.pk
[‡]Sukkur IBA University, Sukkur, Pakistan, iftikhar.kdk@iba-suk.edu.pk
[§]Department of BSRS, Mehran University of Engineering and Technology Jamshoro, Pakistan, fozia.shaikh@faculty.muet.edu.pk
[**]Department of BSRS, Mehran University of Engineering and Technology Jamshoro, Pakistan, anwar.solangi@faculty.muet.edu.pk

discusses reactors related to the aforementioned applications (Fortin & Esselaoui, 1987).

Several studies have examined the behavior of unidirectional and reverse flows of Newtonian fluids in channels (A. A. Bhutto, Ahmed, et al., 2023; A. A. Bhutto, Hussain, et al., 2022; I. A. Bhutto, Bhutto, et al., 2023; Fortin & Esselaoui, 1987). Experimentally investigating the characteristics of single-dimensional flow of a linear fluid in a rectangular channel, the authors found that the flow velocity profiles were well-described by laminar flow theory (Cochrane et al., 1982). Further, Afonso (A. M. Afonso et al., 2011) investigated reverse flows in horizontal channels. He found that the reverse flow was initiated by a small disturbance near the inlet and then developed into a stable vortex. Incompressible laminar fluid flows are a fundamental problem in fluid mechanics studied for decades. The behaviour of these flows in complex domains, which can include obstacles, corners, and curved surfaces, is of particular interest due to its significance for many real-world applications (A. A. Bhutto et al., 2022; A. A. Bhutto et al., 2023; I. A. Bhutto et al., 2023; Iftikhar Ahmed et al.,, 2023; Khokhar et al., 2023). Porous media can also significantly affect fluid flows' behaviour, and understanding the interactions between fluids and porous media is crucial in fields such as geology, environmental engineering, and oil extraction.

The study explores the behaviour of incompressible laminar fluid flows within intricate domains, both with and without porous media (Alazmi & Vafai, 2001; Echendu et al., 2011). Over the precedent decades, progress in state-of-the-art, rapid computing systems has progressed significantly, resulting in the creation of intricately designed numerical algorithms. The practical application of computer simulations to analyze complicated fluid dynamics within a domain containing permeable materials has been widely acknowledged and further enhanced by global institutions(Al-Nimr & Aldoss, 2004). The Computational Fluid Dynamics (CFD) approach is expected to exhibit a particular characteristic owing to its ability to perform constraint-based simulations. Over the last three decades, there has been significant progress in enhancing our knowledge of numerical uncertainties, and the flow nature, such as unsteady, and turbulence. The mathematical modelling of flow behaviour by mixing and separating simultaneously, as well as other modifications, was first initiate by Cochrane et al.,(Cochrane et al., 1981). This was experimentally and numerically solved using the finite difference method.

A few 2D analyses were conducted by (Baloch et al., 1995; A. A. Bhutto, Bhutto, et al., 2023) using the finite element procedure, and Afonso et al., 2008 used the finite volume technique. Mixing and separation in rectangular channels and pipes, whether filled with porous media or not, exhibit a plethora of captivating flow phenomena. These include the appearance of singularities at acute bends, the formation of flow transition. These diverse flow phenomena occur within the same domain, as observed by (A. Afonso et al., 2008; Cochrane et al., 1982; Dharejo et al., 2018; Khokhar, 2018) and (Echendu et al., 2011). Investigated mixing and separating flow of highly elastic fluids using a time-dependent finite element method. Taylor-

Petrov-Galerkin algorithms were utilized due to the elastic nature of the fluids (Hawken et al., 1990). They used the pressure-correction method to achieve second-order accuracy in incompressibility. The researchers simulated Newtonian fluid flow with equal flow rates in both arms, while they simulated viscoelastic flows with the Phan-Thien and Tanner (PTT) constitutive model (Pinho & Oliveira, 2000), which numerically illustrates shear-thinning behaviour and the effect of changing in space between plates. They studied various physical parameters, and flow situations (Pinho & Oliveira, 2000). According to (A. M. Afonso et al., 2011), even creeping flow or limited vanishing inertia can reduce the inertia effect on flow rate. A recent study (Benzenine et al., 2010) used numerical simulations in the same flow domain to study linear and viscoelastic liquids.

This study aims to investigate the behaviour of Newtonian liquid in a medium with non-porous media in both combining and separating configurations, and to gain insights into how vortex size, intensity, and stability are affected by Reynolds number, flow rate, and inertia. The study focuses on the impact of flow rate on vortex formation and behaviour at different Reynolds numbers, flow rate with both equal and unequal, examines the impact of inertia, and power when non-porous materials fill the channel. The study also compares the numerical results with existing literature on inertial effects and pressure differences in channels filled with non-porous materials to corroborate the correctness of the simulation model.

Problem Specification

This study investigates a conjoined geometry, mixing and separating, for both reversed and one-directional flows. The details of the geometry are portrayed in Figure 1(a-b), while Figure. 1(c) illustrates the finite element mesh employed in the analysis. The configuration includes a planar channel with two inlets and two outlets, alienated into two portions via joining of two thin horizontal plates located in the mid plane. Primary focus is on the large, spaced geometry, where the severance space, denoted as β, is three times the height of one arm of the channel (L). The investigation aims to analyze the relationship between the gap width and the flow pattern. The thickness of the plates is described as $\alpha = 0.0254L$ in (Baloch et al., 1995).

The channel length at the inlet and outlet is sufficient to replicate fully developed flow. In order to obtain the flow domain, uniform conformal mapping is used, which is then discretized into triangular elements. The finite element mesh consists of 1328 elements, 2853 nodes, 392 limit bumps, 6469 degrees of freedom, and 763 vertex bumps. A semi-implicit method has been utilized, employing the Jacobi algorithm to obtain a precise solution. The time intervals required for Newtonian problems are typically $\Delta t \leq 0.01$. By executing five iterations for each Jacobi step and maintaining a tolerance level of 10^{-6}, a stable solution has been attained.

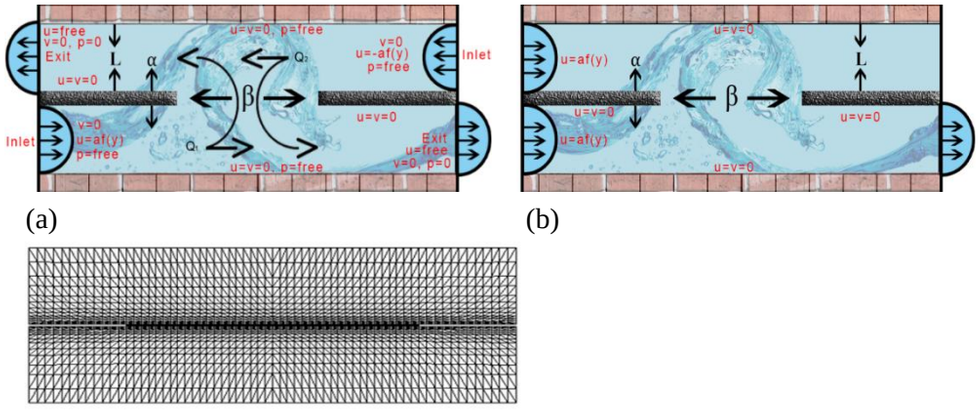

(a) (b)

(c)

Figure 1: Flows are mixed and separated using two inlets and two outlets (reverse flow),

The Initial and Boundary Conditions

In order to fully define the problem, it is essential to specify the initial and boundary conditions. The given Equation (1) is accompanied by a boundary condition expressed in the following format:

$$\frac{\partial v}{\partial t} = \frac{1}{Re}\nabla^2 v - (v.\nabla)v - \nabla p \qquad (1)$$

where

$$v(x,0) = v_0(x) \qquad (2)$$

Subject to

$$\nabla \cdot v_0 = 0 \qquad (3)$$

Monochrome walls of the geometry, and plates implanted in the centre are subjected to no-slip form, where all factors of the velocity field become zero. The steady Poiseuille flow shape, described in Equations (4) and (5), are enacted at both the inlet and outlet sections of the channel in both arms. When there are different flow rates or flow directions, different boundary conditions are used. For simplicity, a pure approximation is made, which has been shown to not reduce the accuracy of the solution and allows for frequent entrance in the flow regions. Obtaining the steady-state solution for constant inertia, transient simulations start from either motionless conditions or two analogous but disparate flows. To speed up calculation times for greater variable values, past steady-state solutions are used as initializing conditions. This applies to materials at both inlets.

$$u(y) = U_m(y-a)(b-y) \quad at\ x = 0 \quad \text{(Bottom left arm)} \qquad (4)$$

$$u(y) = -\mathrm{V}_m\{y-(b+\alpha)\}(2b+\alpha-y) \quad at\ x = 23L \text{ (Top right arm)} \qquad (5)$$

Equations (4) and (5) define a and b as the lower and upper coordinates of the computational domain's wall, with a height of $b-a$, while $\alpha = 0.0254$ represents

the plate's thickness. The channel has a reasonable length of $23L$, ensuring that flow occurs at both the inlets and outlets. Here, L is the specific distance of the channel. The stream at inlet enacted on the bottom left arm, $a = 0$ and $b = 1$. The extreme velocity achieved for equal flow rates in the channel arm center is denoted by $U_m = V_m$whereas for unequal flow rates, U_m and V_m represent the 1 ratio 1.5 and 1 ratio 2, respectively.

At outlet of both the geometries, normal traction-free conditions are maintained to ensure consistency with the fixed pressure $p = 0$. Numerical calculations are exercised to approximate the flow fields, with careful monitoring of the flow regions to ensure that it does not affect the global accuracy of the solutions.

Numerical Method

The present study works governing systems of equations both in Cartesian and cylindrical polar coordinate systems in order to model both steady-state and time-dependent problems. In order to solve these problems, advanced numerical algorithms are employed from the literature. The Newton-Raphson method is the most commonly employed method for obtaining steady-state solutions. The literature contains a variety of algorithms for solving time-dependent problems, including those cited in references (Donea, 1984b). In this study, a multi-stage finite element technique is used, with (Carew et al., 1994) incorporating a compression-correction approach to determine pressure-driven incompressible streams of Newtonian fluids, after an initial explicit method of a Taylor-Galerkin scheme was enhanced. Using the approach proposed by (Donea, 1984a), the algorithm was designed to achieve second-order accurate solutions while also addressing the issue of incompressibility. Although Darcy's term has been introduced into the momentum equation to represent flow through porous materials in the current study, significant progress has been made in improving the model.

Taylor–Galerkin/Pressure–Correction Scheme

This scheme's primary objective formulates an efficient and highly accurate time-stepping structure to capture both transient and steady-state solutions of fluid flow problems. Originally, (Donea, 1984a) presented the algorithm to handle the time-dependent flows of Newtonian liquids while treating the incompressibility condition implicitly. The procedure employs Taylor series expansions to achieve temporal discretization. A two-step predictor-corrector scheme using Lax-Wendroff approximation is used for second-order temporal accuracy of results. It is also possible to capture higher-order accuracy for the derivatives of time and reliable derivatives of space with this algorithm. Compared to Euler-Galerkin and Finite Difference methods, the algorithm demonstrates a significant improvement in accuracy and stability (Donea, 1984a; Hawken et al., 1990). The Pressure-modification technique is a numerical technique originally suggested by (Chorin, 1968) and later refined by Fortin (Fortin & Esselaoui, 1987). It separates the pressure and velocity fields and

uses a linearized momentum analysis to achieve generally second-order accuracy and stability (Peyret et al., 1986).

This method has since evolved into a variety of related techniques, such as the TGPC algorithm (Peyret et al., 1986), which is the numerical algorithm employed in this research. Similar approaches associated to finite difference research work can also be found (Liu & Lax, 2003). For more detailed information on the transient flows of Newtonian fluids (Echendu et al., 2011) can be consulted. However, when it comes to non-Newtonian fluids, the algorithm has been extended experimentally and numerically in both semi-implicit and fully-implicit forms. For flows that are diffusion dominant, the semi-implicit algorithm has proven to be both numerically accurate and computationally efficient, making it a stable choice for specific problems. In the proposed study, the semi-implicit type the TGCP algorithm is applied, and thus, aforementioned approach is demonstrated here.

Time-stepping Scheme with Semi-implicit

There is a numerical method known as semi-implicit time stepping that is used to resolve partial differential equations (PDEs) involving stiff and non-stiff terms at the same time. In this scheme, the non-stiff terms are treated explicitly, while the stiff terms are treated implicitly. A semi-implicit method has been utilized, employing the Jacobi algorithm to obtain a precise solution. The time intervals required for Newtonian problems are typically $\Delta t \leq 0.01$. By executing five iterations for each Jacobi step and maintaining a tolerance level of 10^{-6}, a stable solution has been attained.

Cartesian Co-ordinates

According to a literature review, explicit schemes in numerical simulations can cause computational costs since their slow convergence rate makes large time steps (Δt) difficult to handle. Due to its robustness and ability to enhance correctness, stability, efficiency, and convergence rate at higher time steps, (Baloch et al., 1995; Hawken et al., 1990; M. A. Solangi et al., 2013). It has been observed that while fully implicit numerical algorithms are generally more cost-effective, they may not improve numerical stability. For this study, we have applied a Crank-Nicolson treatment only to the viscous or diffusive and Darcy's module has to obtain the semi-implicit TGCP scheme. In order to maintain accuracy and stability, this approach optimizes computational efficiency.

For solving the Temporal Generalized Convection Problem (TGCP), a semi-implicit methodology is employed for addressing the governing system of equations described in reference (Khokhar, 2018). A Taylor series expansion is used to extend the temporal domain (t_n, t_{n+1}) into a bifurcated process. An initial forward difference scheme is implemented to calculate the speed vector field at an intermediate time step $\left(n + \frac{1}{2}\right)$, based on the primitive variables (v^n, p^n) at $t = t_n$. According to (Van Kan,

1986), this approach adheres to the finite element paradigm. A central difference method is then applied to determine the primitive variables (v^{n+1}, p^{n+1}) at the complete time step $(t = t_{n+1})$. Using the Crank-Nicolson technique, the incompressibility constraint associated with the pressure term is further addressed, resulting in two additional steps.

After acquiring information from the initial step and using the given initial data, the second step involves determining a velocity vector field with non-divergence. It is necessary to obtain a pressure differential at the full-time step $(t = t_{n+1})$ in the third step. Vector field with divergence-free velocity (v^{n+1}) computed in the fourth step by using information gathered in the third step about the pressure difference. Here is the algorithm for integrating the temporal difference into partial detached system of the Darcy-Brinkman equation:

Stage–1a: The speed vector field should not diverge $v^{n+\frac{1}{2}}$ at $n+\frac{1}{2}$ the initial information for the velocity vector field v^n. In addition, pressurep^n at initial level n:

$$\left(\frac{2}{\Delta t}-\frac{1}{2Re}\nabla^2+\frac{1}{2ReD_a}\right)\left(v^{n+\frac{1}{2}}-v^n\right)=\left[\frac{1}{\mathrm{Re}}\nabla^2 v-(v.\nabla)v-\nabla p-\frac{1}{\mathrm{Re\,D}_a}v\right]^n \quad (6)$$

Stage-1b: Calculate transitional non–solenoidal velocity field v^* velocity vector fields $v^{n+\frac{1}{2}}$ calculated at $n+\frac{1}{2}$ instant step and force p^n at distinguish time step n interpreting by using Crank–Nicolson conduct on pressure:

$$\left(\frac{1}{\Delta t}-\frac{1}{2\mathrm{Re}}\nabla^2+\frac{1}{\mathrm{Re\,D}_a}\right)(v^*-v^n)=\left[\frac{1}{\mathrm{Re}}\nabla^2 v-\nabla p-\frac{1}{\mathrm{Re\,D}_a}v\right]^n-(v.\nabla)v^{n+\frac{1}{2}} \quad (7)$$

Stage–2: After resolving the non-divergence free velocity vector v^*, the Poisson equation must be used to calculate the pressure difference $(p^{n+1}-p^n)$ at the complete time step interval (t_n, t_{n+1}), as given below:

In order to calculate the pressure difference $(p^{n+1}-p^n)$ at the complete time step interval (t_n, t_{n+1}) after resolving the non-divergence free velocity vector v^*, the Poisson equation applied, as shown below.

$$\theta\nabla^2(p^{n+1}-p^n)=\frac{1}{\Delta t}\nabla.v^* \quad (8)$$

Stage–3: This paper presents the third and final step of a computational approach for determining speed field v^{n+1} at the end one complete time step $(n+1)$. This process leverages evidence acquired during stages (1b, and 2), in particular the intermediate velocity field v^* and the pressure difference$(p^{n+1}-p^n)$. This step is governed by the following equation:

$$\frac{2}{\Delta t}(v^{n+1}-v^*)=-\nabla(p^{n+1}-p^n) \quad (9)$$

A time step index is denoted by n in this equation. As suggested in previous studies (Baloch et al., 1995; Crank & Nicolson, 1996; M. A. Solangi et al., 2013), the Crank-Nicolson $(\theta = 0.5)$ time discretization scheme is used for this analysis. As part of this scheme, a mid-point temporal step is added to the first temporal fractional stage. As a result of this inclusion, the transition from a first-order projection method

to a second-order projection method is facilitated, resulting in an improved accuracy of the final solution.

Cylindrical Polar Co-ordinates

In numerical simulation the selection of an algorithm depends upon a number of factors, including accuracy, convergence rate, efficiency, and stability. Several studies have demonstrated that semi-implicit methodologies have better convergence rates than explicit methodologies (Baloch et al., 1995; Carew et al., 1994; D. Solangi et al., 2012; M. A. Solangi et al., 2013). Generally, implicit techniques are used to enhance numerical stability without incurring excessive computational costs. These are the specifics of the discrete semi-implicit equations that involve Darcy's component:

Stage–1(a):

$$\left[\frac{2}{\Delta t}M+\frac{1}{Re}\left(\frac{S_{rr}}{2}+\frac{M}{D_a}\right)\right]\left(V_{r,j}^{n+\frac{1}{2}}-V_{r,j}^{n}\right)=\left[-\frac{1}{Re}\{S_{rr}+S_{rz}\}V_{r,j}-J_1^{\dagger}P_k\right]^n-N(V)V_{r,j}^{n}-\frac{1}{ReD_a}MV_{r,j}^{n} \quad (10)$$

$$\left[\frac{2}{\Delta t}M+\frac{1}{Re}\left(\frac{S_{zz}}{2}+\frac{M}{D_a}\right)\right]\left(V_{z,j}^{n+\frac{1}{2}}-V_{z,j}^{n}\right)=\left[-\frac{1}{Re}\{S_{rz}^{\dagger}+S_{zz}\}V_{z,j}-J_2^{\dagger}P_k\right]^n-N(V)V_{z,j}^{n}-\frac{1}{ReD_a}MV_{z,j}^{n} \quad (11)$$

Stage–1(b):

$$\left[\frac{1}{\Delta t}M+\frac{1}{Re}\left(\frac{S_{rr}}{2}+\frac{M}{D_a}\right)\right]\left(V_{r,j}^{*}-V_{r,j}^{n}\right)=\left[-\frac{1}{Re}\{S_{rr}+S_{rz}\}V_{r,j}-J_1^{\dagger}P_k\right]^n-N(V)V_{r,j}^{n+\frac{1}{2}}-\frac{1}{ReD_a}MV_{r,j}^{n} \quad (12)$$

$$\left[\frac{1}{\Delta t}M+\frac{1}{Re}\left(\frac{S_{zz}}{2}+\frac{M}{D_a}\right)\right]\left(V_{z,j}^{*}-V_{z,j}^{n}\right)=\left[-\frac{1}{Re}\{S_{rz}^{\dagger}+S_{zz}\}V_{z,j}-J_2^{\dagger}P_k\right]^n-N(V)V_{z,j}^{n+\frac{1}{2}}-\frac{1}{ReD_a}MV_{z,j}^{n} \quad (13)$$

Stage–2:

$$K(Q^{n+1})=-\frac{2}{\Delta t}\left(J_1V_{r,j}+J_2V_{z,j}\right) \quad (14)$$

Stage–3:

$$M\left({V_{r,j}}^{n+1}-{V_{r,j}}^{*}\right)=\frac{\Delta t}{2}{J_1}^{\dagger}(p^{n+1}-p^{n}) \quad (15)$$

$$M\left({V_{z,j}}^{n+1}-{V_{z,j}}^{*}\right)=\frac{\Delta t}{2}{J_2}^{\dagger}(p^{n+1}-p^{n}) \quad (16)$$

$S=\int\left\{\frac{\partial\phi_i}{\partial x}\frac{\partial\phi_j}{\partial x}+\frac{\partial\phi_i}{\partial y}\frac{\partial\phi_j}{\partial y}\right\}d\Omega$ is a momentum diffusion matrix,

$J_1=\int\frac{\partial\psi_i}{\partial x}\phi_j\,d\Omega$ and $J_2=\int\frac{\partial\psi_i}{\partial y}\phi_j\,d\Omega$ are divergence/pressure gradient matrix and $J=(J_1,J_2)$ and $K=\int\left\{\frac{\partial\psi_{ki}}{\partial x}\frac{\partial\psi_{kj}}{\partial x}+\frac{\partial\psi_{ki}}{\partial y}\frac{\partial\psi_{kj}}{\partial y}\right\}d\Omega$ is a stiffness matrix. Here, † is matrix transpose. V^n, V^*, V^{n+1} are nodal directions of speed field, p^n, p^{n+1} is stress,

and Δt is time period (t_n, t_{n+1}). V_j^n, is a nodal velocity vector at time t_n , V_j^* is an intermediate non-divergence-free velocity vector and $V_j^{n+1}$is a divergence-free velocity vector at time stept_{n+1}. In calculations p_k^n is a pressure vector and $Q^{n+1} = p_k^{n+1} - p_k^n$ is a pressure difference vector.

Results and Discussion

The present study numerical solutions for Newtonian flows that combine and separate within a channel containing non-porous media. The analysis explores various aspects, including flow stream patterns, vortex development, and pressure differences caused by alterations in flow rates and directions. To illustrate different combinations, Figure. 1. (a-c) depict variations in flow rates and directions.

Non-Porous Media-Filled Channel With Newtonian Fluid Flow Mixing And Separation (G_1)

Figure. 1-a in the depicts the behaviour of a Newtonian fluid in a channel that includes non-permeable modes in both combining and separating configurations. To erect two identically sized inlet and outlet channel arms on either side of the division, plates with a separation gap width of β are introduced into the computational domain. β is a specific length that corresponds to the top of a firth arm of the channel. The plate wideness, α, is fixed at $0.0254\,L$, and the channel length is selected to be sufficiently long to ensure fully established stream at the domain's entry and exit. The research examines the influence of inertia, vortex size, and power when non-porous materials fill the channel. The results obtained in this study are contrasted by the existing literature on inertial effects and pressure differences in channels filled with non-porous materials, which is illustrated in Figure. 10 and 11.

Flow Rate Equal to (1, 1)

The stream rate in each outlet arm is identical, as specified by the notation (1, 1). To gain insight into the impact of inertia, it is required to analyze the flow of a Newtonian liquid and the corresponding stream rates. Figure 2 depicts the mathematical outcomes for increasing Reynolds numbers ranging from $1 \leq R_e \leq 200$. The results revealed that the liquid reacted to the occurrence of the space and promptly disintegrated, with the flow amalgamation in mutually higher and lower exit portions of the geometry. At $R_e = 15$, the emergence of recirculation approximately the walls has initiated in both branches of a conduit. At Reynolds number (say $R_e = 15$), the two vortices produced close to top wall, and bottom channel arms strike and blend into one another, covering the central space of the domain.

This solitary vortex expands in magnitude and takes on a distinct eddying pattern. By employing the same methodology to growth the rate of Re, the expansion of the severity of grown vortices becomes more discernible in the vicinity of the grab of the attached plates in the upper and lower canal arms, as proved in Figure.2 (at

$R_e = 30$ to 150) by exhibiting symmetry in relation. These self-governing swirling masses of fluid near the periphery undergo an enlargement in magnitude as the value of Reynolds number rises. At precisely $R_e = 100$, these vortices stabilize, expand in size, and realign themselves along the wall. The disturbance caused by the convergence of two vortices in the centre gap amplifies and broadens horizontally as it shifts its position. These vortices also initiate a counter current, intensify in size, and give rise to two additional vortices within the primary vortex that are positioned symmetrically to each other (at $R_e = 200$).

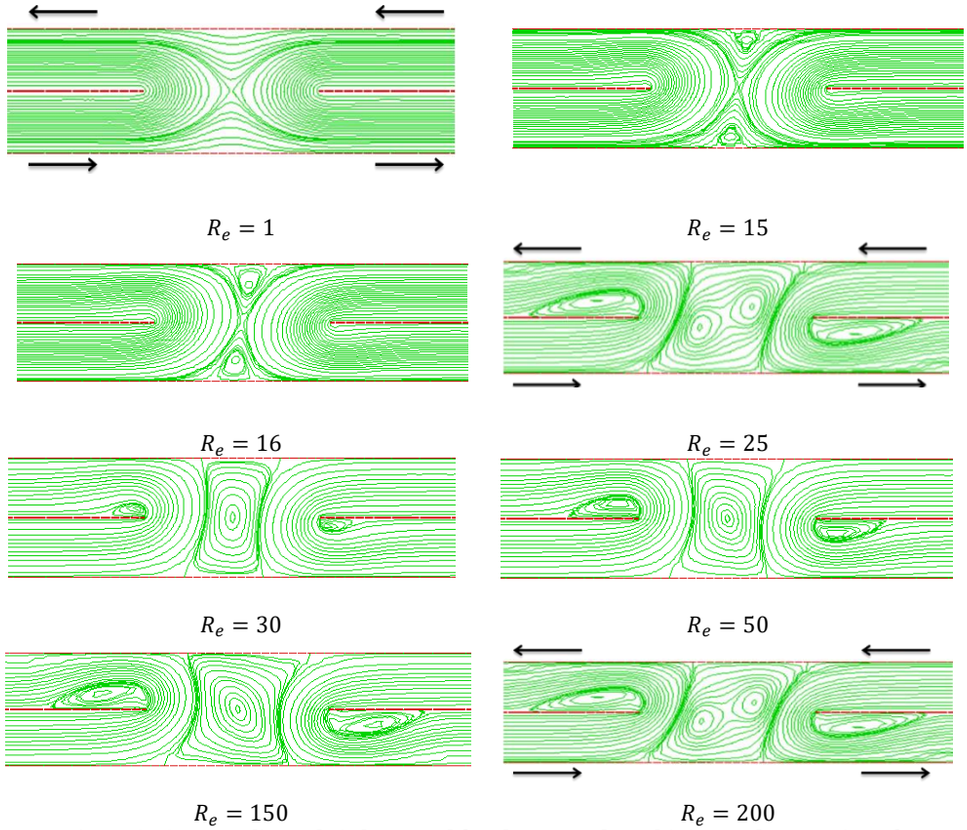

Figure 2: A streamline role is bestowed for the merged combining and separating of Newtonian fluid streams for a stream rate that is equal (1, 1) in both channel limbs and rises from maximum to minimum

The twin swirling masses situated close to the boundary verge to assume a more deviant and extended form in the horizontal and vertical planes. Enhancing the Reynolds number results in the amplification of the magnitude and potency of the central and rearward vortices. However, at very great Reynolds numbers, the vortices seem to break up into multiple smaller vortices. Under the flow conditions of equal

(1, 1) rate, the dominant counter current vortices in the centre gap of the region obstruct the flow, resulting in a reversed flow (at $R_e = 15$). Effective combining of the liquids in the central gap has been witnessed.

Flow Rate Unequal to (1, 1.5)

This study presents numerical consequences of Newtonian fluid in a conduit with unequal flow rates (1, 1.5), as illustrated in Figure. 3. We analyse the case in which U_m equals V_m, and the fluids flow in each channel arm according to the 1:1.5 ratio. We explore the effects of varying Reynolds numbers ($1 \leq R_e \leq 200$) on the flow dynamics in the same domain while keeping the flow rate ratio fixed. In order to achieve this, we begin our simulations with $R_e = 1$ and then increase the upper channel arm flow rate. The perturbation causes the flow to reverse down channel arm because of the downriver propagation of the disturbance. Lower channel arm shows weak vortex activity at $R_e = 1$, particularly at the sharp edge near the exit flow. The behaviour of Newtonian flows in a channel under growing

Reynolds numbers is investigated in the same way as for the equivalent (1, 1) flow rate case. There is an additional vortex beside the fence in the top channel arm of the area wall at $R_e = 25$. With increasing Reynolds numbers, the vortex near the insert plate lies flat, adjusts its position, and grows deeper and more stable while being inclined with the wall. Interestingly, in the case of the same flow rate, the vortex seems on either side of the wall of the higher channel, whereas in the case of quicker flow rate, it appears on both walls. A vortex occurs in the lower channel arm from one side only near the central plate at $R_e = 10$, whereas a second vortex appears very late at $R_e = 50$ on the other side. Figure. 3 ($R_e = 100\ to\ 200$) shows how the vortex near the boundary wall grows and forms an eddy as the Reynolds number increases, increasing recirculation intensity and pushing more toward the middle separation gap. In the top channel arm downstream of $R_e = 200$, another vortex appears. In all three locations, vortices developed in a similar manner in terms of their growth, intensity, stability, and symmetry. In addition, as was witnessed in the instance of equal flow rate, increasing the Reynolds number increases vorticity size, strength, and stability, with both unidirectional and reversed flows occurring.

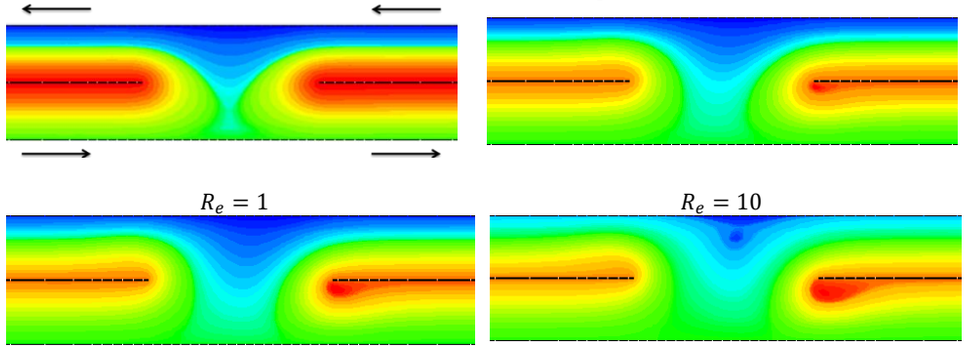

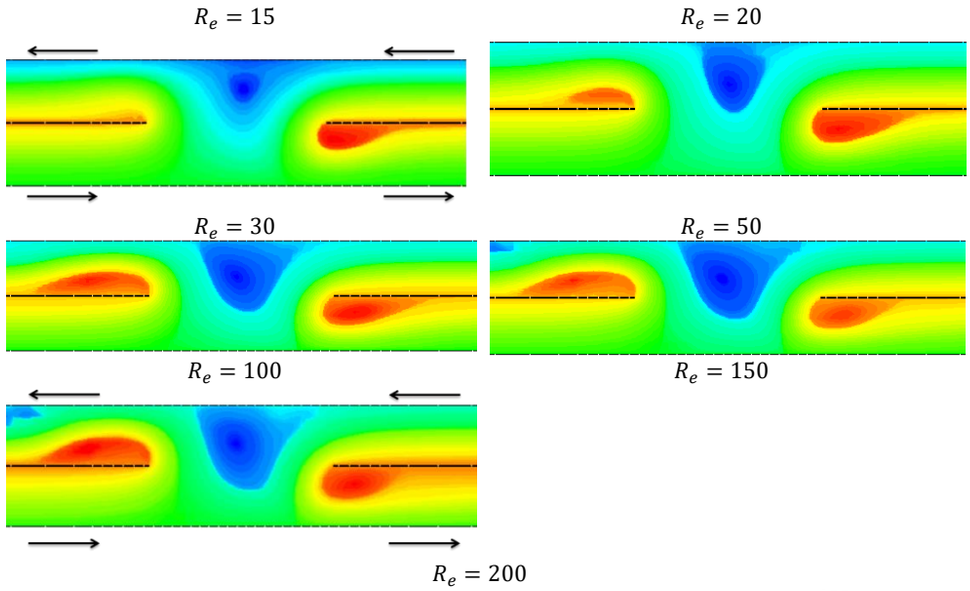

Figure 3: Streamline patterns illustrating the combined mixing and separation of Newtonian fluid flow in a channel under unequal (1, 1.5) flow rate conditions in both arms.

Flow Rate Unequal to (1, 2)

In this case, we observe the stream of a Newtonian liquid in a channel including two arms, where the fluid passes through the lower and upper arms in a ratio of 1:2. As a result, fluid flows twice as fast through the upper arm as through the lower arm. As shown in Figure. 4, the flow behavior for a non-porous media channel is illustrated where the fluid flows unequally (1:2) in both arms of the channel. In order to determine the effect of Reynolds number on the flow pattern in this configuration, we perform numerical simulations for both arms within the range of $1 \leq R_e \leq 200$. In the numerical simulations, streamline shapes are designed at equal interludes in two flow areas: one-directional and inverted. In the blending area, outlines are fabricated from the division line to the plate positioned at the center, whereas in the one-way current region, outlines are fabricated from the wall of the channel to the division line.

An upper arm of a channel with a dual flow rate produces notable results. It was observe that vortex activity began to develop near the modify of the verge of the central plate in the lowest canal arm when a unit Reynolds number used at the beginning of the experiments. In the lower channel, the fluid was push down by the double flow rate in the upper arm. In response to increasing Reynolds number, the vortex became larger and skewed towards right flow direction. A second vortex developed in the top channel arm only when Reynolds numbers reached 50 and above. At higher Reynolds numbers, the vortex appeared late and developed even later. In addition, this late development pushed flow downwards in the lower arm, specifically interior space of the area, at $R_e = 50$. Computational inertial effects were more visible

when Reynolds number was increased. In the channel, all three vortices recirculated and grew in size, adjusting their position by lying horizontally. Despite maintaining symmetry in their size and shape, these vortices grew both vertically and horizontally. In addition to the flow rate (1, 1.5), we now discuss the flow rate (1, 2), resulting in a more dramatic change in flow structure. Similar to (1, 1.5), vortices were observed in the computational domain. Among these locations are the upper egress, lower departure besides the included plates, and the middle separation gap. Additionally, increased Reynolds number led to larger, stronger, and more intense vortices, as seen previously in (1, 1.5) for unequal flow rates. As a result of these vortices, eddies formed, causing fluids in the central gap to mix and separate. The numerical simulations accurately capture fluid flow behavior in all three configurations, indicating that they accurately reflect experimental results.

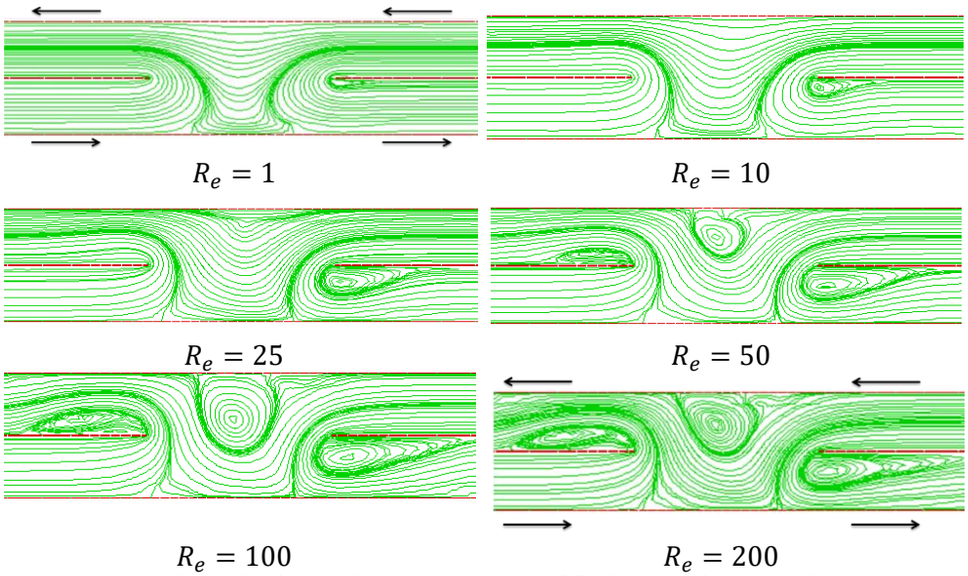

Figure 4: Streamline roles for combining and parting of fluid stream for unequal (1, 2) stream rate in mutually arms of channel, improving Re from maximum to minimum.

Effects of Flow Rate

The numerical simulation results for varying flow rates illustrated in Figure 3 and Figure 4, specifically unequal flows [(1, 1.5) and (1, 2)], within a non-porous channel. Both unequal flow rates exhibit reversed and unidirectional flows within the channel. Notably, altering the flow rate in the upper arm triggers early vortex advancement associated to the equal flow rate case. The influences of inertia are intensified with an increase in Reynolds number. In the lower arm, unidirectional flow is suppressed when the stream rate in the upper arm is changed from unequal (1, 1.5)

to equal (1, 2). Separation and mixing are mainly conducted in the down arm or in the central space of the area.

Stimulus of unequal flow rate on flow structure

The Newtonian fluid flows in nonporous channels undergo dramatic changes when flow rates are unequal. Numerical simulations are used to investigate this phenomenon, with the results presented in Figures. 3 & 4. According to the study, no evidence of completely reversed flows is observed because of increasing Reynolds number. As flow rates increase, unidirectional flow intensifies, while reversed flow persists. When stream rates increase in the topmost arm of a channel, unidirectional flow intensifies, and vortices grow near one end. As a result, the strength of the vortex besides the mid plate in the lowest arm of the channel decreases and is repressed near the other end. It is also evident that the twin vortex that appeared in the middle space of the partition gap of the plate undergoes changes in site. A movement can be observed from the bottom channel arm to the upper channel arm, possibly through a gap located near the upper wall of the channel, and then gradually moves upward by impelling the flow in the lower channel arm. The present research indicates that an increase in Reynolds number results in a decrease in both size and strength of vortex patterns, resulting in their splitting into smaller vortices. It has been followed that unequal flow rates deliver vortex growing primarily top canal arm, with negative mark of vortex development in the smallest channel arm at the central of the boundary because of the relative flow rates. Furthermore, for initial rates of Re, the altering flow rates in the upper channel arm have been found to cause the vortex to disappear near its edge on its left. However, when Re reaches up to 50, there is very late activity of the third vertex. A separation gap is also observed to be a place where flows mix and separate, however the mixing does not appear to be similar to that which is observed in equal stream rates. Because of these findings, we have gained an understanding of the complex dynamics of fluid flow at varying Reynolds numbers and flow rates, as well as valuable insight into the behavior of vortices in such systems.

Differences in pressure caused by flow rates

This study illustrates in Figure.5 the scaled pressure versus Reynold numbers (inertia) relationship of Newtonian fluids in a merged mixing and unravelling geometry. In this study, Reynolds $1 \leq R_e \leq 200$ numbers ranging from were analysed, for all relative flow rates. The following method is used to produce non-dimensional scaled max and min pressure values for flow rates $1 \leq p_s \leq 2.8013$ of equal and unequal amplitudes. The present numerical scheme was utilized. According to the non-dimensional scaled pressure values for equal and unequal flow rate conditions (1, 1.5) and (1, 2), the values were $1 \leq p_s \leq 5.6551$ and$1 \leq p_s \leq 8.4396$, respectively. The study also examines the effect of increasing Re verses non-dimensionally scaled pressure differences for all three comparative flow rates. The non-dimensional scaled pressure difference calculated using the formula $p_s =$

$\frac{Re \times \Delta p_{max}}{(\Delta p_{max} O \ at \ Re=1)}$. In this case, p_s represents the scaled pressure difference, Re represents the Reynolds number calculated as $Re = \frac{\rho v L}{\mu}$ and ∇p_{max} represents the non-dimensional pressure difference. Overall, the results of the work offer valuable perceptions into the relationship between non-dimensional scaled pressure and Reynolds number in Newtonian fluids when mixing and separating are combined. It is important to note that these findings have significant implications for various industrial applications involving fluid flow, such as chemical processing and pipeline transportation. According to the results of the study, increasing relative flow rates leads to an increase in pressure difference, as illustrated in Figure. 5. There is an increase in pressure for each of the three flow conditions with increasing relative flow rates. The differences between the three flow rates in increasing order of Reynolds number can clearly be seen in Figure. 5 when comparing the three flow rates. The pressure changes only slightly when Re is lower than 50. The pressure changes significantly at higher values of Re (100 to 200). Increasing Re alongside the correlated stream rates in the high arm of a canal results in rising effect on difference pressure.

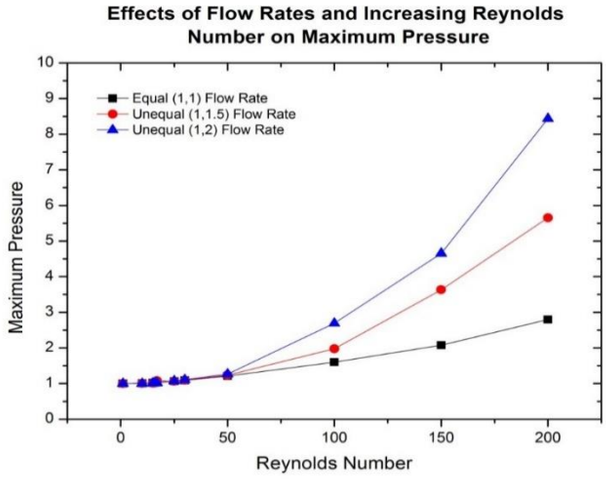

Figure 5: In a non-porous medium channel filled with a maximum-scaled pressure, inertia increases as flow rate is altered.

The combining and Separation of Newtonian fluid streams in a channel fulfilled with a non-porous medium (G_2)

There are two inlets in the experimental setup. According to Figure. 1(a), the streams are in inverse directions, with the two other outlets on the right side of the lower channel arm and on the left side of the upper channel arm. According to Figure. 1(b), the flow in G2 is unidirectional, with two inlets on the left side in respectively arm and only one outlet on the right in the lower arm. The idea of this study is to investigate the flow structure and differentiation in pressure between the arms of

unidirectional Newtonian fluids under modifying flow rates. As in the previous section, the domain was filled without porous media, and the same procedure was applied for the presentation of streamline functions. In order to better understand how inertia effects on flow and pressure variance, Newtonian fluids were examined at varying relative flow rates.

Flow rate unequal to (1, 1)

For equal flow rates in both channel arms, Figure. 6 presents numerical solutions of Newtonian fluid flows. The right side of the computational domain shows two large vortices downstream of the upper arm. One vortex is located on the sharp edge of the central plate, on the right side of the channel, while the other vortex is further downstream. Figure. 6 illustrates the size of the vortex located on the sharp edge of the upper arm of the channel for Reynolds numbers of 20, 30, 50, 100, and 150. Near the central plate and towards the exit of the bottom channel arm, an additional inertial effect is observed. A weak vortex is observed moving horizontally toward the blockage at $R_e = 200$ after the two vortices merge into one larger vortex. A unidirectional flow leads to mixing in the parting gap and lower arm of the channel. In systems where mixing and parting are critical factors, these findings have important implications for understanding fluid flow behaviour in channels.

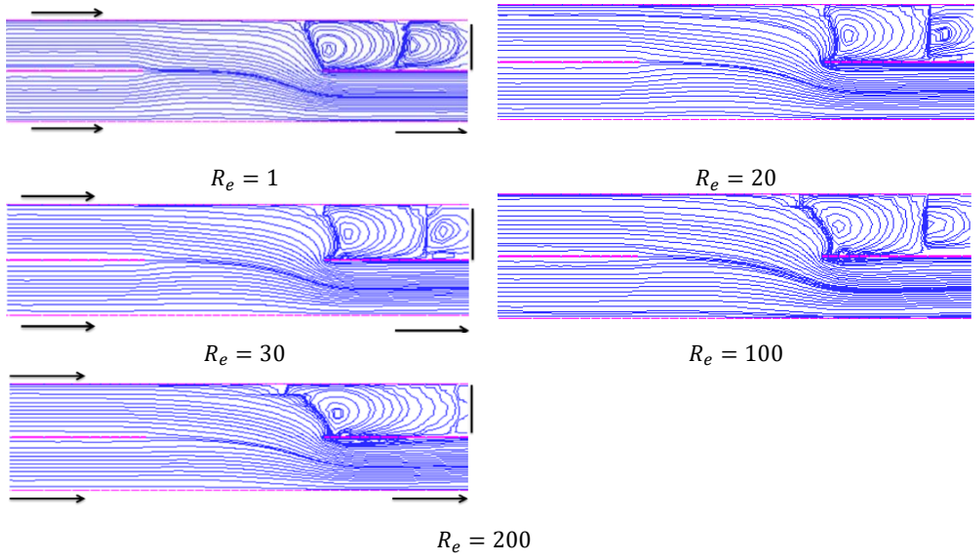

Figure 6: A gradual increase from top to bottom. An analysis of streamline functions for Newtonian fluids flowing in both arms of a channel at equal (1, 1) rates.

Flow rate unequal (1, 1.5)

This study presents quantitative data for the same domain at Reynolds numbers ranging from 1 to 200, as shown in Figure. 7. Flow rates have been improved in the higher channel in order to observer changes in inertia and blending of fluids. At an equal stream rate, the observed effects are almost identical to those at an equal flow rate, except for the development of a vortex near the inserted plate at the exit in the lower arm. Compared to the vortex that appeared at an equal flow rate, which discussed earlier, this vortex is stronger and larger. Nevertheless, the similar mixing impacts were observed as in the case of equal flow rates.

The development of vortex activity has been witnessed at lower Reynolds numbers as well. During the rise in Reynolds number at $R_e = 150$, a whirlpool manifested in close proximity to the centrally positioned plate on its right side. There is evidence that the whirlwind established in the silent arm has been pushed downriver to the silent arm downstream of the top canal arm. With growing stream rate, two vortices tend to merge more quickly. Despite this, the same mixing effects were observed at an equal stream rate. The numerical results obtained in this study have been compared with those made by Cochrane et al. (1981), and very similar. Comparison is shown in Figure. 10.

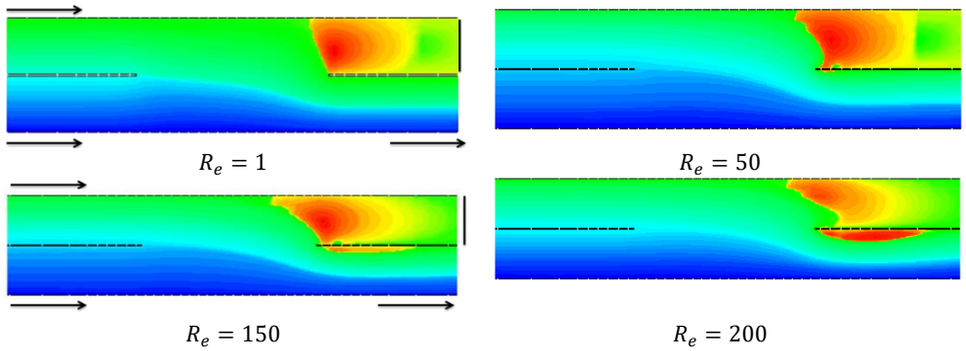

Figure 7: Improving R_e from top to bottom. The development of streamlined functions for combined mixing and separation of fluid flow in two arms of the channel with unequal flow rates (1, 1.5)

Flow Rate is nequal (1, 2)

The purpose of this study was to investigate the effects of mixing and inertia on fluid flow in a channel. By doubling the fluid stream rate in the higher arm of the channel, we observed the resulting behaviour. A numerical simulation of the same unidirectional domain is shown in Figure. 8. At higher Reynolds numbers, we observed similar effects across the range of Reynolds numbers tested (from 1 to 150). As Reynolds number 100 approached, dual turbulences appeared in the silent corner, which merged earlier than at higher Reynolds numbers. The results were also compared with those in a previous section G_1 where we discussed two flow rates in the same situation. The lower channel arm, close to the centrally positioned plate, also

showed a weak vortex influence. We conclude that the fluid stream rate in the upper arm of the channel has a significant impact on mixing and inertia effects.

The results of our research indicate that when $R_e = 150$, the fluid is pushed towards a quiet turn due to a twice stream rate in the upper arm of the channel. In accordance with our numerical scheme, this phenomenon highlights the stability of the developed code. A vortex is also observed to form neighbouring the mid of plate, which grows and adjusts its perception on the plate as it moves toward the exit. Eventually, when $R_e = 150$, the merged vortex splits into two separate vortices that then grow in size. In this scenario, mixing effects are comparable to those examined in section G_1.

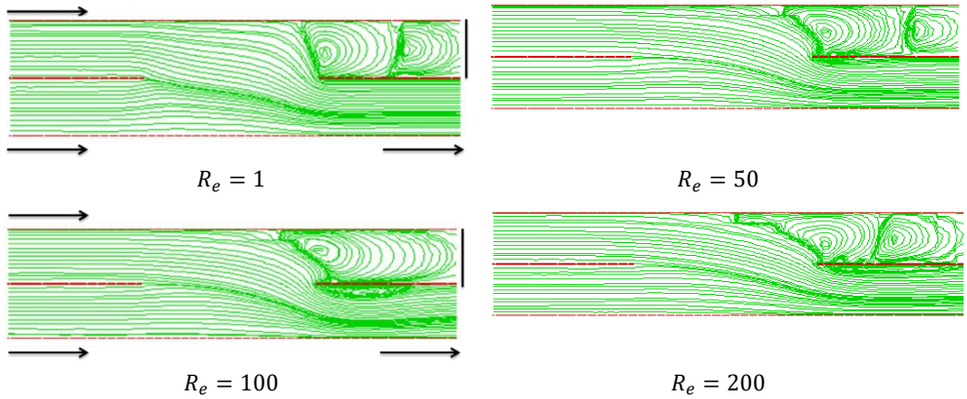

Figure 8: Fluid stream in a canal occupied with nonporous media with unequal flow rates in equally arms, increasing from top to bottom, for unidirectional flows Newtonian fluid.

Effects of stream rate

We present numerical simulations of Newtonian fluid for different flow rates in Figure. (7) and (8), where the flow rates considered are (1, 1.5) and (1, 2). In early stages, changing stream rates significantly affected the development of vortices and determined the direction of fluid flow in silent corners of the domain towards the blockage upstream. It is observed in the silent corners of the channel that two vortices merge early when there is an unequal stream rate in both canal arms. In unidirectional flow, an unstable vortex has also been observed near the central position plate. The upper channel arm has also perceived to exhibit more inertia due to changes in flow rates. Combined vortices tend to split into two again as the Reynolds number increases. In spite of this, we have observed similar mixing effects when flow rates are equal. As a result, we find that flow rate significantly affects the development of vortices and mixing in non-porous media, which has implications for a variety of applications, including chemical reactors and oil recovery.

Analysis the Outcome of Growing Inertia and Flow Rates On Pressure

This article presents a non-dimensional scaled plot of pressure difference versus Reynolds number. For all comparative flow rates, Reynolds numbers range between 1 to 200. We analysed three different stream rates to obtain non-dimensional scaled values for extreme and least pressure differences. For identical stream rate, the values are $1 \leq p_s \leq 2.4255$, for unequal (1,1.5) flow rate, the values are $1 \leq p_s \leq 2.5365$, and for unequal (1,2) flow rate, the values are $1 \leq p_s \leq 2.6374$. As discussed earlier, Pressure differences have been scaled in the same manner for all three relative flow rates. As Reynolds numbers increase for Newtonian fluid flows under the three relative flow conditions, the pressure increases linearly. This behavior contrasts with that of G_1, whose relative flow rates are shown in Figure. 5. The pressure conflict changes smoothly in this unidirectional flow situation as compared to the reversed flow situation discussed earlier. It is clear from a comparison of Figures. 5 and 9 that there is a significant difference in pressure behavior. As shown in the Figure. 9, a lower value of inertia does not elicit any significant changes. A gradual increase in inertia, however, is accompanied by a significant change in Reynolds number, particularly as the Reynolds number progresses from lower to higher values. Unidirectional flows result in uniform flow rate curves. As shown in Figure. 9 (from $R_e = 100\ to\ 200$), pressure displays more inertia effects when reversed, particularly for higher pressures. Pressures range from 1 to 3 units within this range. Pressure varies little between $R_e = 1\ to\ 50$, but changes significantly between $R_e = 100\ to\ 200$.

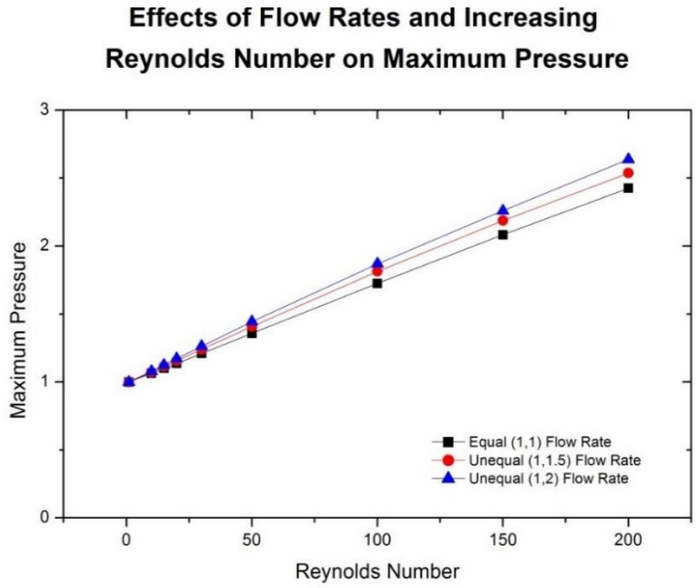

Figure 9: The determined mounted pressure and improving inertia of a channel filled with nonporous material were associated at various flow rates.

The present study did not observe the impact of Weissenberg number on the flow rate of the domain without any porous media present in the channel. Figure. 10 depicts unidirectional and inverted streams with both equal and unequal stream rates in both arms of the channel. The mathematical results of this study are compared to the experimental results of (Cochrane et al., 1982) in Figure. 10. The Figure indicates that both arms of the channel have an equal flow rate, indicating that the current experimental findings are in line with this examination.

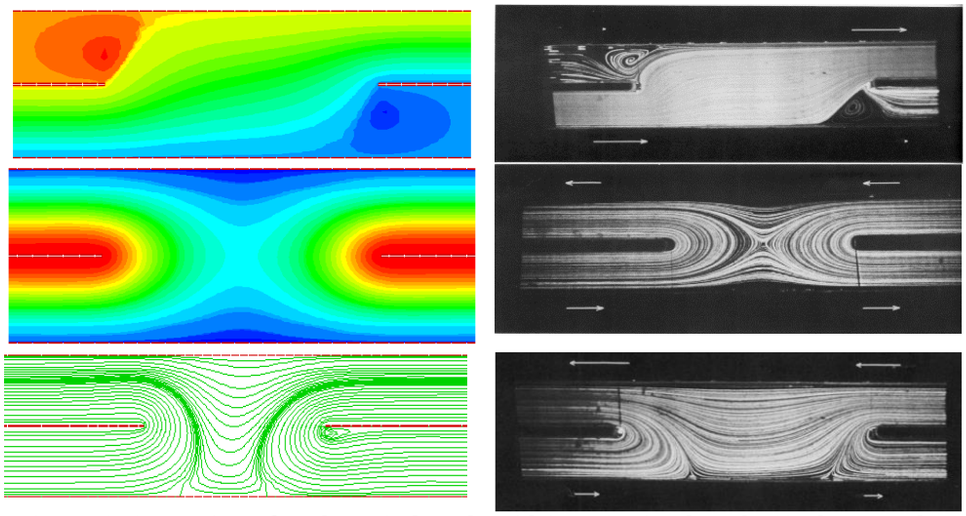

Figure 10: Comparison of mathematical results with investigational results (Cochrane et al., 1982).

The channel streams are characterized by varying flow directions and fluctuating flow rates as illustrated in Figure. 11. This Figure illustrates the experimental results that are in accordance with the predictions derived from our present analysis. Accordingly, Figure. 11 illustrates unequal flow rates (1, 2) in both arms of a channel system. Our numerical analysis generated results at a $R_e = 1$ and a width parameter (W) of 0.17, whereas the experimental results were obtained at $R_e = 0.75$ and a width parameter (W) of 0.17. The current numerical results also indicate unidirectional flow at $R_e = 1$, which is consistent with the experimental results at $R_e = 1$ and $W = 0.23$. We found a high degree of similarity between our study and the experimental investigation conducted by [6] at $R_e = 1$.

Moreover, the reversed flow observed in our study confirms the results reported by [6]. It is important to note, however, that a significant distinction lies in the presence of a dual stream rate in the upper arm of the channel in our study. Consequently, the fluid is forced into the medium gap of the lower arm, as illustrated in Figure. 11. A significant finding from the experiment described in [6] is that a double flow rate was observed in the lower channel arm. This indicates that fluid is being forced into the middle gap of the upper channel arm.

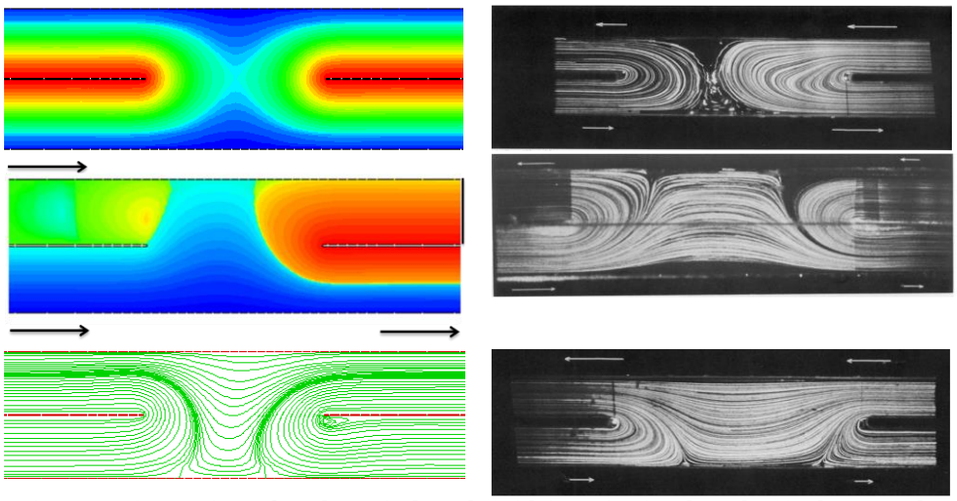

Figure 11: Comparison of mathematical results with investigational results (Cochrane et al., 1981)(Cochrane et al., 1982)

Conclusion

Taylor-Galerkin/Pressure-Correction primeval variable finite element algorithms have emerged as reliable and accurate computational tools for predicting complex and steady fluid flows in channels containing Newtonian fluids. The results of in-depth investigations, which have involved varying flow directions, flow rates, and Reynolds numbers, have revealed a variety of bifurcations, including vortex development, eddy formation, and pressure differences. In this study, it has been demonstrated that altering the flow direction and rate has a substantial impact on flow structure and pressure distribution, with a higher Reynolds number resulting in a stronger vortex. The findings of this study contribute to our understanding of fluid dynamics and have practical implications for the design and optimization of fluid flow systems.

Recommendations

The findings also indicate that the algorithm holds potential for optimizing fluid flow systems. It offers valuable insights into the impacts of factors like flow direction, rate, and Reynolds number on flow structure and pressure distribution. These discoveries carry substantial implications for industries like aerospace, automotive, and chemical engineering, where efficient and cost-effective operations heavily depend on fluid flow system optimization.

Funding Source

This research did not receive any specific grant from funding agencies in the public, commercial, or not-for-profit sectors.

Conflict of interest

The authors have no conflict of interest.

References

Afonso, A., Alves, M. A., Poole, R. J., Oliveira, P. J., & Pinho, F. T. (2008). Viscoelastic low-Reynolds-number flows in mixing-separating cells. *Proceedings of the 6th International Conference on Engineering Computational Technology*.

Afonso, A. M., Alves, M. A., Poole, R. J., Oliveira, P. J., & Pinho, F. T. (2011). Viscoelastic flows in mixing-separating cells. *Journal of Engineering Mathematics*, *71*, 3–13.

Al-Nimr, M. A., & Aldoss, T. K. (2004). The effect of the macroscopic local inertial term on the non-Newtonian fluid flow in channels filled with porous medium. *International Journal of Heat and Mass Transfer*, *47*(1), 125–133.

Alazmi, B., & Vafai, K. (2001). Analysis of fluid flow and heat transfer interfacial conditions between a porous medium and a fluid layer. *International Journal of Heat and Mass Transfer*, *44*(9), 1735–1749.

Baaijens, F. P. T. (1998). J. Non-Newtonian Fluid Mech. *Mixed Finite Element Methods for Viscoelastic Flow Analysis: A Review*, *79*, 361.

Baloch, A., Townsend, P., & Webster, M. F. (1995). On the simulation of highly elastic complex flows. *Journal of Non-Newtonian Fluid Mechanics*, *59*(2–3), 111–128.

Benzenine, H., Saim, R., Abboudi, S., & Imine, O. (2010). Numerical simulation of the dynamic turbulent flow field through a channel provided with baffles: comparative study between two models of baffles: transverse plane and trapezoidal. *Journal of Renewable Energies*, *13*(4), 639–651.

Bhutto, A. A., Ahmed, I., Rajput, S. A., & Shah, S. A. R. (2023). *The effect of oscillating streams on heat transfer in viscous magnetohydrodynamic MHD fluid flow*.

Bhutto, A. A., Bhutto, I. A., Soomro, M. A., Kashif, U. A. K., & Bhutto, I. A. (2023). Numerical Analysis of Inertia Effects on Pressure and Flow Patterns in Unidirectional and Reversed Newtonian Fluid Flows within a Channel. *VFAST Transactions on Mathematics*, *11*(2), 42–62.

Bhutto, A. A., Harijan, K., Hussain, M., Shah, S. F., & Kumar, L. (2022). Numerical simulation of transient combustion and the acoustic environment of obstacle vortex-driven flow. *Energies*, *15*(16), 6079.

Bhutto, A. A., Hussain, M., Feroz, S., Shah, A., & Harijan, K. (2022). Computation of Vortex Driven Flow Instability through Unsteady RANS and Scale Resolving Simulation. *Institute of Space Technology*, *12*(1), 14–22.

Bhutto, A. A., Shah, S. F., Khokhar, R. B., Harijan, K., & Hussain, M. (2023). *To Investigate Obstacle Configuration Effect on Vortex Driven Combustion Instability*.

Bhutto, I. A., Bhutto, A. A., Khokhar, R. B., Soomro, M. A., & Shaikh, F. (2023). *The effect of uniform and exponential streams on Magnetohydrodynamic flows of viscous fluids.*

Carew, E. O., Townsend, P., & Webster, M. F. (1994). Taylor-Galerkin algorithms for viscoelastic flow: application to a model problem. *Numerical Methods for Partial Differential Equations*, *10*(2), 171–190.

Chorin, A. J. (1968). Numerical solution of the Navier-Stokes equations. *Mathematics of Computation*, *22*(104), 745–762.

Cochrane, T., Walters, K., & Webster, M. F. (1981). On Newtonian and non-Newtonian flow in complex geometries. *Philosophical Transactions of the Royal Society of London. Series A, Mathematical and Physical Sciences*, *301*(1460), 163–181.

Cochrane, T., Walters, K., & Webster, M. F. (1982). Newtonian and non-Newtonian flow near a re-entrant corner. *Journal of Non-Newtonian Fluid Mechanics*, *10*(1–2), 95–114.

Crank, J., & Nicolson, P. (1996). A practical method for numerical evaluation of solutions of partial differential equations of the heat-conduction type. *Advances in Computational Mathematics*, *6*(1), 207–226.

DHAREJO, K., SHAIKH, H., SHAH, B., & BALOCH, A. (2018). Least square Galerkin Finite Element study of Newtonian Fluids Flow through channel with fixed Rectangular Single Baffle. *Sindh University Research Journal-SURJ (Science Series)*, *50*(2), 215–220.

Donea, J. (1984a). A Taylor–Galerkin method for convective transport problems. *International Journal for Numerical Methods in Engineering*, *20*(1), 101–119.

Donea, J. (1984b). Recent advances in computational methods for steady and transient transport problems. *Nuclear Engineering and Design*, *80*(2), 141–162.

Echendu, S. O. S., Belblidia, F., Tamaddon-Jahromi, H. R., & Webster, M. F. (2011). Modelling with viscous and viscoplastic materials under combining and separating flow configurations. *Mechanics of Time-Dependent Materials*, *15*, 407–428.

Fortin, M., & Esselaoui, D. (1987). A finite element procedure for viscoelastic flows. *International Journal for Numerical Methods in Fluids*, *7*(10), 1035–1052. https://doi.org/10.1002/FLD.1650071004

Hawken, D. M., Tamaddon-Jahromi, H. R., Townsend, P., & Webster, M. F. (1990). A Taylor–Galerkin-based algorithm for viscous incompressible flow. *International Journal for Numerical Methods in Fluids*, *10*(3), 327–351.

Iftikhar Ahmed Bhutto a, Ilyas Khan b, Muhammad Furqan c, Abeer H. Alzahranid d, Afaque Ahmed Bhutto e, A. S. f. (2023). S0360319923033323. *International Journal of Hydrogen Energy*.

Khokhar, R. B. (2018). *Numerical Modelling of Mixing and Separating of Fluid Flows through Porous Media*.

Khokhar, R. B., Bhutto, A. A., Siddiqui, N. F., Shaikh, F., & Bhutto, I. A. (2023). *Numerical analysis of flow rates, porous media, and Reynolds numbers affecting the combining and separating of Newtonian fluid flows*.

Liu, X.-D., & Lax, P. D. (2003). Positive schemes for solving multi-dimensional hyperbolic systems of conservation laws II. *Journal of Computational Physics*, *187*(2), 428–440.

Peyret, R., Taylor, T. D., & Berger, S. A. (1986). Computational methods for fluid flow. *Physics Today*, *39*(7), 70–71.

Pinho, F. T., & Oliveira, P. J. (2000). Analysis of forced convection in pipes and channels with the simplified Phan-Thien–Tanner fluid. *International Journal of Heat and Mass Transfer*, *43*(13), 2273–2287.

Solangi, D., Shaikh, H., Khokhar, R. B., & Baloch, A. (2012). Numerical study of Newtonian blood flow through a plaque deposited artery. *Sindh University Research Journal (Science Series)*, *45*(01), 79–82.

Solangi, M. A., Khokhar, R. B., & Baloch, A. (2013). A fem study for non-newtonian behaviour of blood in plaque deposited capillaries: Analysis of blood flow structure. *Mehran University Research Journal of Engineering and Technology*, *32*(2), 277–282.

Van Kan, J. (1986). A second-order accurate pressure-correction scheme for viscous incompressible flow. *SIAM Journal on Scientific and Statistical Computing*, *7*(3), 870–891.

Xia, B., & Sun, D.-W. (2002). Applications of computational fluid dynamics (CFD) in the food industry: a review. *Computers and Electronics in Agriculture*, *34*(1–3), 5–24.